

Imaging features of hepatic sarcomatous carcinoma on computed tomography and gadoxetic acid-enhanced magnetic resonance imaging

Kyo-won Gu,¹ Young Kon Kim,¹ Ji Hye Min,¹ Sang Yun Ha,² Woo Kyoung Jeong¹

¹Department of Radiology and Center for Imaging Science, Samsung Medical Center, Sungkyunkwan University School of Medicine, Seoul, Republic of Korea

²Department of Pathology, Samsung Medical Center, Sungkyunkwan University School of Medicine, Seoul, Korea

Abstract

Purpose: To determine the imaging features of hepatic sarcomatous carcinoma including sarcomatous intrahepatic cholangiocarcinoma (S-ICC) and sarcomatous hepatocellular carcinoma (S-HCC) on computed tomography (CT) and gadoxetic acid-enhanced magnetic resonance imaging (MRI).

Materials and methods: Twenty-four patients with pathologically confirmed S-ICCs ($n = 13$), S-HCCs ($n = 7$), sarcomatous carcinoma ($n = 2$), carcinosarcoma ($n = 1$), and sarcomatous combined HCC-CC ($n = 1$) (size range 2.1–23 cm, mean 8.3 cm) underwent gadoxetic acid-enhanced MRI ($n = 20$) and/or dynamic CT ($N = 24$). Underlying chronic hepatitis or cirrhosis was found in 17 patients. Two reviewers evaluated morphology, signal intensity, and enhancement features of tumors based on a consensus.

Results: Lobulated contour was observed in 15 tumors (62.5%); the rest were round or oval masses. During dynamic imaging, S-ICCs showed poor enhancement ($n = 10$ on CT; $n = 7$ on MRI) or initial thin-rim enhancement with/without progressive enhancement ($n = 3$ on CT; $n = 6$ on MRI). S-HCCs and the other four tumors showed a thin or thick enhancement pattern on both CT and MRI. T2 bright signal intensity similar to fluid was found in 10 tumors. Target appearance on hepatobiliary phase and diffusion-weighted imaging was seen in two S-ICCs and two S-HCCs. Of 18 surgically resected tumors, 17 showed vascular invasion and/or thrombosis in histology and 12 in CT and MRI. Ten tumors were accompanied by intrahepatic metastasis or

tumor seeding and 19 patients had recurrence or progression of tumors during follow-up.

Conclusion: Hepatic sarcomatous carcinoma including S-HCC and S-ICC generally presents minimal rim-like arterial enhancement or extreme hypovascularity on CT and gadoxetic acid-enhanced MRI with a high frequency of T2 bright area due to extensive necrosis and vascular invasion.

Key words: Sarcomatous carcinoma—Cholangiocarcinoma—Hepatocellular carcinoma—Gadoxetic acid—Magnetic resonance imaging

Sarcomatous carcinomas are a very rare variant type of hepatic tumor, defined as a malignant tumor containing an intimate mixture of carcinomatous (either hepatocellular or cholangiocellular) and sarcomatous elements [1, 2]. Thus, sarcomatous changes can occur in both hepatocellular carcinoma (HCC) [1, 2] and intrahepatic cholangiocarcinoma (ICC) [3–6]. The incidence of sarcomatoid changes based on surgical and autopsied cases has been reported to be 3.9%–9.4% of HCCs and approximately 4.5% of ICCs [1, 2, 7, 8]. Sarcomatous change in HCC or ICC is defined as “sarcomatous HCC (S-HCC)” or “sarcomatous ICC (S-ICC)” in the World Health Organization (WHO) classification of tumors [9]. This entity is differentiated from hepatic carcinosarcoma, which contains both hepatocellular carcinoma and a sarcoma component but lacks the spindle-shaped cells seen in S-HCC or S-ICC [4, 10, 11].

In the literature, S-HCC, S-ICC, and hepatic carcinosarcoma have been reported with limited imaging findings [11–14]. The prognosis is known to be poor in patients with S-HCC or S-ICC as a result of the significantly higher frequency of recurrence or metastasis compared with typical HCC or ICC [1, 5, 15–17]. To the best of our knowledge, no reports are available on the imaging features of S-HCC or S-ICC or hepatic carcinosarcoma in a large case series using state-of-the-art MRI. Since gadoxetic acid, a hepatocyte-specific magnetic resonance (MR) contrast agent, is now widely used to assess hepatic tumors, awareness of the imaging features of HCC or ICC with sarcomatous changes or hepatic carcinosarcoma on gadoxetic acid-enhanced MRI is important for patient care and to avoid errors in diagnosis and management. With these concepts in mind, we conducted this study to determine the imaging features of hepatic sarcomatous carcinoma including S-HCC or S-ICC on dynamic CT or gadoxetic acid-enhanced MRI in a large case series.

Materials and methods

Patients

This retrospective study was approved by the relevant institutional review board, and informed consent was waived. We retrospectively searched our hospital's pathological database for liver tumors between November 2011 and June 2015 using the search terms “*sarcomatous*” or “*sarcomatoid*.” Of 2220 patients who had undergone hepatic surgery or percutaneous biopsy for liver mass, the search identified 25 consecutive patients who had sarcomatous hepatic tumors based on pathology. One patient was excluded because the hepatic mass was considered to be metastasis from pancreatic rhabdomyosarcoma. The final cohort included 24 patients (15 men, 9 women; age range 44–74 years; mean age 58.1 years). Before treatment, all patients had undergone CT examination and 20 had also undergone gadoxetic acid-enhanced MRI.

Reference standard

The reference standard for sarcomatous hepatic tumors was based on histopathological examination of surgical specimens for 18 patients or percutaneous biopsy for six patients who were not candidates for surgery because of extrahepatic tumor seeding ($n = 3$) or intrahepatic metastasis with portal vein thrombosis ($n = 3$). The average time interval between MR examination and surgery was 13 days (range 2–23 days). Operations included tumorectomy ($n = 1$), segmentectomy ($n = 4$), bisegmentectomy ($n = 1$), and hemihepatectomy ($n = 12$). Histopathological factors that were assessed for each tumor were as follows: gross type; histological type; cell type; fibrous capsule and septum formation;

vascular invasion; bile duct invasion; presence of fat, necrosis, or hemorrhage; presence of satellite nodule or intrahepatic metastasis; and presence of extrahepatic seeding or lymph node metastasis. Microscopically, the tumors were mostly composed of pleomorphic spindle cells with numerous mitoses (sarcomatous component), and moderately to poorly differentiated adenocarcinoma (S-ICC) or HCC component with trabecular arrangement (S-HCC). Tumors were assessed immunohistochemically using antibodies directed against cytokeratin (CK) AE1/AE3, vimentin, hepatocyte antigen, smooth muscle actin, CD34, CD31, C-kit, CD68, and S100 to differentiate sarcomatous tumors from ordinary HCC or ICC. Based on the histopathologic findings and immunohistochemical results, tumors were diagnosed as S-ICC, S-HCC, carcinosarcoma, sarcomatous carcinoma, or sarcomatous combined hepatocellular and cholangiocarcinoma (S-HCC–CC). Immunoreactivity of carcinomatous component or sarcomatous component to cytokeratin (epithelial feature) and vimentin (mesenchymal feature) was used to distinguish S-ICC from carcinosarcoma, in which only molecular features of mesenchyme were expressed in the sarcomatous component [4].

CT and MR examination

Multiphasic (unenhanced, arterial, portal venous, and equilibrium phases) CT was conducted with either a 40-MDCT scanner (Brilliance 40; Philips Healthcare) or a 64-MDCT scanner (Aquilion 64; Toshiba Medical and LightSpeed VCT 64, GE Healthcare). The scanning parameters were 120 kVp, 189–200 mAs, 5 mm slice thickness with an increment (overlap) of 2.5 mm, a table speed of 26.5–39.37 mm/rotation (pitch 0.828–1.07), and a single-breath-hold helical acquisition of 4–6 s, depending on liver size. Hepatic arterial phase scanning began 30–40 s after the injection of 110 or 120 mL of the non-ionic iodinated contrast agent iopamidol (Iopamiro 300, Bracco) at a rate of 3–4 mL/s, by means of a bolus-triggered technique (120 kVp; 40–60 mA; monitoring frequency from 12 s after the contrast injection, 1 s; trigger threshold, 100 HU in the descending aorta; delay from trigger to initiation of scan, 18 s). The portal and equilibrium phases of scanning began 70 and 180 s after the injection of the contrast agent, respectively.

MRIs were acquired using a 3.0-T whole-body MRI system (Intera Achieva; Philips Healthcare, Best, The Netherlands) equipped with a dual-source parallel radiofrequency transmission system and quadrature body coil. Baseline MRI included T1-weighted turbo field-echo in-phase and opposed sequence (TR/first echo TE, second echo TE, 10/2.3 [in-phase], 3.45 [opposed-phase]; flip angle, 15°; matrix size, 256 × 194; bandwidth, 434.3 Hz/ pixel), breath-hold multishot T2-

weighted sequence with an acceleration factor of 2 (1796/70; flip angle, 90°; matrix size, 324 × 235; bandwidth, 258.4 Hz/pixel), and respiratory-triggered single-shot heavily T2-weighted sequence with an acceleration factor of 2 (1802/160; flip angle, 90°; matrix size, 252 × 254; bandwidth, 420.9 Hz/pixel) with 5 mm section thickness and a field of view of 32–38 cm.

For gadoteric acid-enhanced imaging, unenhanced, arterial phase (AP, 20–35 s), portal phase (PVP, 60 s), 3-min late-phase, and 20-min hepatobiliary (HBP) images were obtained using a T1-weighted 3D turbo field-echo sequence (enhanced T1 high-resolution isotropic volume examination; eTHRIVE, Philips Healthcare) (3.1/1.5; flip angle, 10°; matrix size, 256 × 256; bandwidth, 724.1 Hz/pixel) with a 2 mm section thickness and a field of view of 32–38 cm. The measured voxel size was 1.5 × 1.5 × 4.0 mm, and reconstructed voxel size was 1.17 × 1.17 × 2.0 mm. Contrast agent was automatically administered intravenously at a rate of 1 mL/s for a dose of 0.025 mmol/kg body weight using a power injector, followed by a 20-mL saline flush.

Diffusion-weighted single-shot echo-planar imaging with simultaneous respiratory triggering was performed using TR/TE 1600 ms/70 ms. TR was matched in each patient to respiratory cycle length prior to gadoteric acid enhancement. Scanning parameters were as follows: b value 0, 100, and 800 s/mm²; spectral presaturation with inversion recovery for fat suppression; matrix size, 100 × 100; acceleration factor of SENSE, 2.0; field of view, 35 × 35 cm; number of excitations, 4; slice thickness, 5 mm; slice gap, 1 mm; and 33 axial slices. Depending on patient respiratory efficiency, acquisition time for the sequence was 3–4 min. The apparent diffusion coefficient was calculated using a mono-exponential function with b values of 100 and 800 s/mm².

Image analysis

All MRI and CT images were evaluated by consensus of two gastrointestinal radiologists J.H.M and Y.K.K with 5 and 13 years of experience in liver MRI, respectively. All images were evaluated using a Picture Archiving and Communication System (PACS, GE Medical Systems Integrated Imaging Solutions, Mt. Prospect, IL, USA) with an optimal window setting adjustment for each patient. Although there were minor discrepancies between the readers in assigning signal intensity of tumors, common consensus was easily reached during an additional reading session. The following imaging features were evaluated: (1) shape of tumors (lobulated, round, or oval); (2) attenuation of tumor on unenhanced and contrast-enhanced CT; (3) signal intensity of tumors relative to liver parenchyma on precontrast T1-weighted images (T1WI), T2-weighted images (T2WI), gadoteric acid-enhanced images (AP, PVP, 3-min late, and HBP), and b-800 diffusion-weighted image (DWI); (4) presence

of arterial hyperenhancement, followed by washout on portal venous and/or 3-min delayed phase; (5) arterial rim enhancement (thin or thick rim), followed by progressive and concentric fill-in during dynamic imaging; (6) presence of target appearance that consisted of central enhancement and peripheral hypointense rim on 10 or 20-min HBP or target appearance that consisted of central hypointense area and peripheral hyperintense rim on b-800 DWI [18, 19]; and (7) presence of ancillary features including tumor capsule, liver surface retraction, biliary dilatation periphery to tumor, invasion of portal vein or hepatic vein, and intra- and extrahepatic metastasis (i.e., seeding nodule and lymph node metastasis). The bright hyperintense area on T2WI was considered positive when there were areas with signal intensity higher than that of the spleen. The hypointense area on T2WI was considered positive when there were areas with signal intensity lower than that of the liver parenchyma [19]. Breath-hold multishot T2WI was used for qualitative assessment. Classification as thin- or thick-rim enhancement was based on <10% of the tumor diameter. The presence of capsule was considered positive when PVP or 3-min late-phase images demonstrated a peripheral rim of smooth hyperenhancement around the tumor [20].

Results

Baseline clinical and histological characteristics

Tables 1 and 2 show clinical and pathologic features of the study population and tumors included in the study, respectively. Seventeen patients had liver cirrhosis ($n = 8$) or chronic hepatitis ($n = 9$) associated with viral hepatitis B ($n = 12$), viral hepatitis C ($n = 2$), or of unknown origin ($n = 3$). Histologically, 13 tumors (54.2%) were S-ICC and 7 tumors (29.2%) were S-HCC. The remaining four tumors were considered sarcomatous carcinoma ($n = 2$), carcinosarcoma ($n = 1$), and S-HCC-CC ($n = 1$). Seven of eight S-ICCs that were surgically resected had extensive necrosis (20%–80% of the tumor area; mean, 51.4%). Six S-HCCs showed necrosis ranging from 1 to 80% of the tumor area (mean, 31%) in pathology. The capsule was identified in five S-HCCs. The carcinosarcoma, sarcomatous carcinoma, and S-HCC-CC showed necrosis of 60%, 40%, and 15% of the tumor area, respectively. Of 18 tumors that were surgically resected, 17 showed macrovascular ($n = 7$; 4 S-ICCs, 1 S-HCC, sarcomatous carcinoma, and carcinosarcoma) and/or microvascular ($n = 17$; 7 S-ICCs, 6 S-HCCs, two sarcomatous carcinoma, carcinosarcoma, and S-HCC-CC) invasion on pathology. One patient with S-ICC (#6) had previous history of transarterial chemoembolization for HCC 3 years ago before diagnosis of S-ICC. None of the other patients underwent adjuvant therapy before surgery. Six patients who did not undergo surgery received chemotherapy ($n = 5$) or

Table 1. Clinical findings of 24 patients with 24 hepatic sarcomatous tumors

No.	Sex	Age	Histologic diagnosis	Confirm	Underlying disease	AFP	CA19-9	Follow-up result	Total follow-up period (months)
1	M	65	Favor sarcomatous ICC	Biopsy	CH-B	3.6	11.25	Progress, 2 months	3
2	M	70	Sarcomatous ICC	Resection	CH-B	N/A	22.44	Recur, 2 months	3
3	F	48	Sarcomatous ICC	Resection	Hepatolithiasis	1.8	7.28	Recur, 18 months	35
4	M	45	Sarcomatous ICC	Biopsy	CH-B	2.8	10384.0	Progress, 4 months	5
5	F	46	Favor sarcomatous ICC	Biopsy	Normal liver	1.9	N/A	Progress, 1 month	2
6	M	69	Sarcomatous ICC	Resection	Unknown, HCC s/p TACE	2.7	25.81	Recur, 1 month	1
7	F	54	Sarcomatous ICC	Resection	CH-B	1.6	11.34	Recur, 6 months	26
8	M	74	Sarcomatous ICC	Resection	CH-C	1.8	6.07	Recur, 4 months	12
9	M	57	Favor sarcomatous ICC	Biopsy	Normal liver	6.17	2.0	Progress, 2 months	2
10	M	51	Sarcomatous ICC	Resection	CH-B	5.1	11.71	Recur, 1 month	3
11	M	69	Sarcomatous ICC	Biopsy	Normal liver	N/A	N/A	Progress, 1 month	2
12	F	61	Sarcomatous ICC	Resection	Normal liver	1.6	886.51	Recur, 4 months	4
13	M	53	Sarcomatous ICC	Resection	CH-B	93.8	10.55	Recur, 1 month	3
14	F	56	Sarcomatous HCC	Resection	CH-C	4.3	1.0	Recur, 1 month	2
15	F	62	Sarcomatous HCC	Resection	CH-B	35.6	1.81	Free	26
16	M	64	Sarcomatous HCC	Resection	CH-B	814.8	11.51	Free	19
17	M	59	Sarcomatous HCC	Resection	CH-B	2.7	N/A	Follow-up lost	
18	F	64	Sarcomatous HCC	Resection	CH-B	1.3	N/A	Free	20
19	M	52	Sarcomatous HCC	Resection	Unknown	3.1	20.73	Recur, 1 month	2
20	M	44	Sarcomatous HCC	Resection	CH-B	11.1	6.64	Recur, 3 months	24
21	F	66	Carcinosarcoma	Resection	Normal liver	3.4	16.38	Follow-up lost	
22	F	48	Sarcomatous carcinoma	Resection	Normal liver	1.5	19.81	Recur, 2 months	1
23	M	68	Sarcomatous carcinoma	Biopsy	Unknown	13.7	8.72	Progress, 1 month	3
24	M	50	Sarcomatous HCC-CC	Resection	CH-B	2.8	N/A	Recur, 4 months	5

Duration for progression or recurrence is an interval between pathologic diagnosis and progression or recurrence on follow-up imaging evaluation. Tumor progression was determined based on the RECIST criteria

ICC intrahepatic cholangiocarcinoma; HCC hepatocellular carcinoma; HCC-CC combined hepatocellular and cholangiocarcinoma; CH-B chronic viral hepatitis B; CH-C chronic viral hepatitis C; AFP alpha-fetoprotein; CA19-9 carbohydrate antigen 19-9; N/A not available

Table 2. Histologic characteristics of 18 resected sarcomatous carcinoma

Gross features of surgical specimen	
Size (cm)	8.3 ± 6.1 ^a
Necrosis (%)	
S-ICC	20–80, mean; 51.4 ^b
S-HCC	1–80, mean; 31 ^b
Carcinosarcoma	60
S-carcinoma	40
S-HCC-CC	15
Microscopic features	
Microvascular or lymphovascular invasion	
Positive	17 (94.4)
Negative	1 (5.6)
Portal vein invasion or thrombosis	
Positive	7 (38.9)
Negative	11 (61.1)
Intrahepatic metastasis	
Positive	2 (11.1)
Negative	16 (88.9)
Grade	
I / well differentiated	0 (0.0)
II / moderately differentiated	0 (0.0)
III / poorly differentiated	5 (27.8)
IV / undifferentiated	13 (72.2)

Data in the parenthesis in “microscopic features” are the percentages of patient

S-ICC sarcomatous intrahepatic cholangiocarcinoma; S-HCC sarcomatous hepatocellular carcinoma; CS carcinosarcoma; S-carcinoma sarcomatous carcinoma; S-HCC-CC sarcomatous combined hepatocellular and cholangiocarcinoma

^a Data are mean value ± standard deviation

^b Mean values are calculated only when necrosis is present

radiotherapy ($n = 1$). Tumors in all six patients showed progression during follow-up.

CT and MRI features

Imaging features of HCCs are summarized in Table 3. The tumor diameters ranged from 2.1 to 23 cm (mean 8.3 cm, median 6.0 cm), including 13 S-ICCs that ranged from 3.7 to 23.0 cm (mean 8.3 cm, median 7.0 cm) and 7 S-HCCs that ranged from 2.1 to 22.0 cm (mean 8.3 cm, median 6.0 cm). Regarding morphology, 15 tumors (62.5%) showed lobulated or wavy contours (Fig. 1), 5 (4 S-HCCs and one S-HCC-CC) were oval shaped, and 3 S-HCCs were round shaped (Fig. 2). On dynamic CT images, the majority of S-ICCs ($n = 10$, 76.9%) showed hypovascularity with poor enhancement and the remaining three showed barely perceptible initial thin-rim enhancement with mild progressive enhancement during portal and 3-min delayed phases (Fig. 1). On gadoteric acid-enhanced MRI, 6 S-ICCs showed initial thin-rim enhancement with mild progressive fill-in enhancement pattern during dynamic phases in five (Fig. 1), and the remaining 7 S-ICCs showed poor enhancement. S-HCCs showed thin or thick enhancement pattern on both CT ($n = 7$) and MRI ($n = 5$) (Fig. 2). Thus, no S-HCC showed definitive homogeneous arterial hyperenhancement followed by washout on PVP and 3-min late-phase

Table 3. Summary of imaging characteristics of 24 sarcomatous tumors

	CT enhancement (<i>n</i> = 24)			MR enhancement (<i>n</i> = 20)			Target sign (<i>n</i> = 20)	T2WI (<i>n</i> = 20)	
	Poor	Thin rim	Thick rim	Poor	Thin rim	Thick rim		HBP/ DWI	Bright SI component
S-ICC (<i>N</i> = 13)	10	3 (3)		7	6 (5)		2	6 / 2 ^a	1
S-HCC (<i>N</i> = 7)		4	3		2	3	2	2	1
CS or S-ca (<i>N</i> = 3)		3 (3)			1 (1)			1	
S-HCC-CC (<i>N</i> = 1)			1			1		1 ^a	

S-ICC sarcomatous intrahepatic cholangiocarcinoma; S-HCC sarcomatous hepatocellular carcinoma; CS carcinosarcoma; S-ca sarcomatous carcinoma; S-HCC-CC sarcomatous combined hepatocellular and cholangiocarcinoma; HBP hepatobiliary phase; DWI diffusion-weighted image; T2WI T2-weighted image; SI signal intensity. Numbers in parentheses represent the number of tumors showing progressive fill-in enhancement pattern during dynamic phases

^a Data indicate diffuse brightness on T2WI

image. Two S-ICCs and two S-HCCs showed a target appearance on both HBP images and DWI (Figs. 1, 2). Of the remaining four sarcomatous tumors, three (one carcinosarcoma and two sarcomatous carcinomas) showed initial thin-rim enhancement with mild progressive enhancement similar to S-ICC, and the remaining S-HCC-CC was seen as a well-defined oval-shaped mass showing relatively thick peripheral arterial hyperenhancement, mimicking S-HCC.

All 24 tumors were hypointense on T1WI and hyperintense relative to liver parenchyma on T2WI. Bright signal intensity similar to that of cyst or hemangioma on T2WI was seen in 6 S-ICCs (Fig. 3), 2 S-HCCs, 1 sarcomatous carcinoma, and 1 S-HCC-CC, all of which presented necrosis (1–80% of the tumor area) in histology. Two S-ICCs (necrosis 37.5% and 20%) and 1 S-HCC-CC (necrosis 15%) were seen as diffuse bright signal intensity on T2WI (Fig. 4). A central area of dark signal intensity on T2WI was noted in one each S-ICC and S-HCC. This area translated into central delayed enhancement on HBP and a darker central area on DWI, which was responsible for the target appearance. In pathology, the T2 darker area was considered to be abundant fibrosis with necrosis (S-ICC) and without necrosis (S-HCC).

On preoperative imaging of all 24 tumors, 10 tumors were accompanied by intrahepatic metastasis (*n* = 5) or tumor seeding (*n* = 5). Portal vein thrombosis or direct invasion on both CT and MRI was observed in 8 S-ICCs, 1 S-HCC, 1 sarcomatous carcinoma, carcinosarcoma, and S-HCC-CC. Two S-ICCs presented as subcapsular necrotic mass with rupture into the perihepatic space resulting in multifocal peritoneal tumor seeding (Fig. 5). Biliary dilatation periphery to tumor was seen in two S-ICCs. Hepatic surface retraction was seen in three S-ICCs.

Of 24 patients, 13 patients who received surgery showed recurrence (72.2%), six showed progression, three were progression free during 12 or 14 months after surgery, and two were lost to follow-up according to the RECIST criteria [21]. Tumor recurrence or progression manifested as local recurrence at resection margin (*n* = 5), intrahepatic metastasis (*n* = 9), peritoneal

seeding (*n* = 9), and metastasis to lymph node (*n* = 5), lung (*n* = 3), or bone (*n* = 1)

Discussion

Our study demonstrated that sarcomatous hepatic tumors generally present hypovascularity seen as rim enhancement or non-enhancement on AP imaging of CT or MRI, in accordance with previous reports [4, 5, 10, 12, 14, 22–24]. This might be mostly attributed to increased tumor necrosis because the sarcomatous component consists of poorly differentiated cells that grow rapidly with the neovasculature unable to adequately supply the fast-growing malignant cells, resulting in necrosis [12, 23–25]. Thus, sarcomatous change causes HCC or ICC to lose classic imaging features. The pathogenesis of sarcomatous tumor has not yet been clarified. Systemic chemotherapy, transcatheter arterial embolization-induced necrosis, and direct viral replication have been reported to be involved in sarcomatous transformation of carcinoma [8, 15, 17, 26–28]. The role of hepatolithiasis and infection has also been proposed [7, 29]. In our study population, 17 patients (70.8%) had underlying chronic hepatitis or cirrhosis and one had hepatolithiasis.

Classically, mass-forming ICCs manifest as a non-encapsulated lobulated mass that shows arterial rim enhancement, followed by progressive and concentric fill-in during dynamic imaging. Because of the histologic characteristics of ICC, which consists of a central area containing a fibrotic stroma and a peripheral vascular-rich cellular area, ICCs tend to show central enhancement with a peripheral hypointense rim, or target appearance, on ultra-delayed imaging using gadopentate dimeglumine or HBP imaging of gadoxetic acid [19]. This is also true for DWI, where the central hypointensity might be attributable to dense collagen seen as T2 dark signal intensity (T2 blackout effect) or loose fibrosis, whereas necrosis is seen as T2 bright signal intensity causing increased diffusivity [18]. In our study, only two S-ICCs showed a target appearance on HBP and DWI. On AP of CT or MRI, only six tumors showed barely

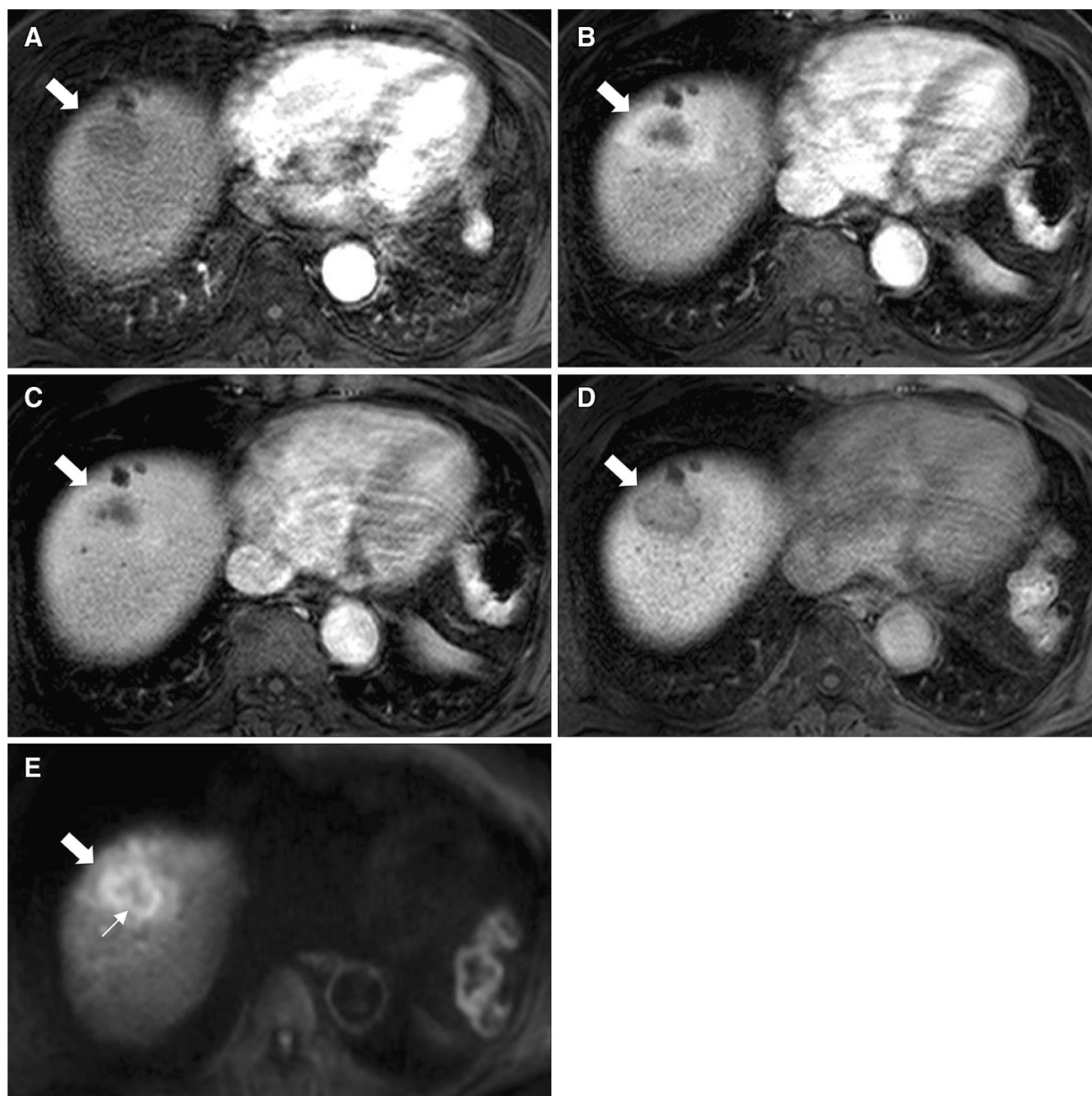


Fig. 1. A 4.0-cm sarcomatous intrahepatic cholangiocarcinoma with tumor necrosis (45%) in a 74-year-old man with hepatitis C-induced chronic hepatitis. Axial fat-suppressed T1-weighted 3D gradient echo images obtained during arterial phase (**A**), portal venous phase (**B**), and 3-min delayed phase (**C**): tumor with lobulated contour (*arrows*) shows poor arterial enhancement with progressive fill-in enhancement. **D** On the

20-min hepatobiliary phase image, the tumor (*arrow*) is seen as a target appearance of central enhancing area with peripheral hypointense rim. **E** The tumor (*arrow*) has a target appearance of a central dark area (*small arrow*) and peripheral hyperintense area on single-shot echo-planar diffusion-weighted imaging at $b = 800 \text{ s/mm}^2$.

perceptible rim enhancement and the others showed diffuse hypoattenuation or hypointensity. Given that all but one of the surgically proven S-ICCs had extensive necrosis (20%–80% of tumor area) in histology, extensive necrosis appears to be the main factor contributing to alterations in the classic enhancement of ICC.

In the same manner, no S-HCCs fit the typical HCC enhancement pattern of arterial hyperenhancement and washout. Although three tumors showed a relatively thick peripheral hyperenhancing rim on AP of CT and MRI, they showed a pattern more similar to the ICC enhancement pattern due to a central non-enhancing

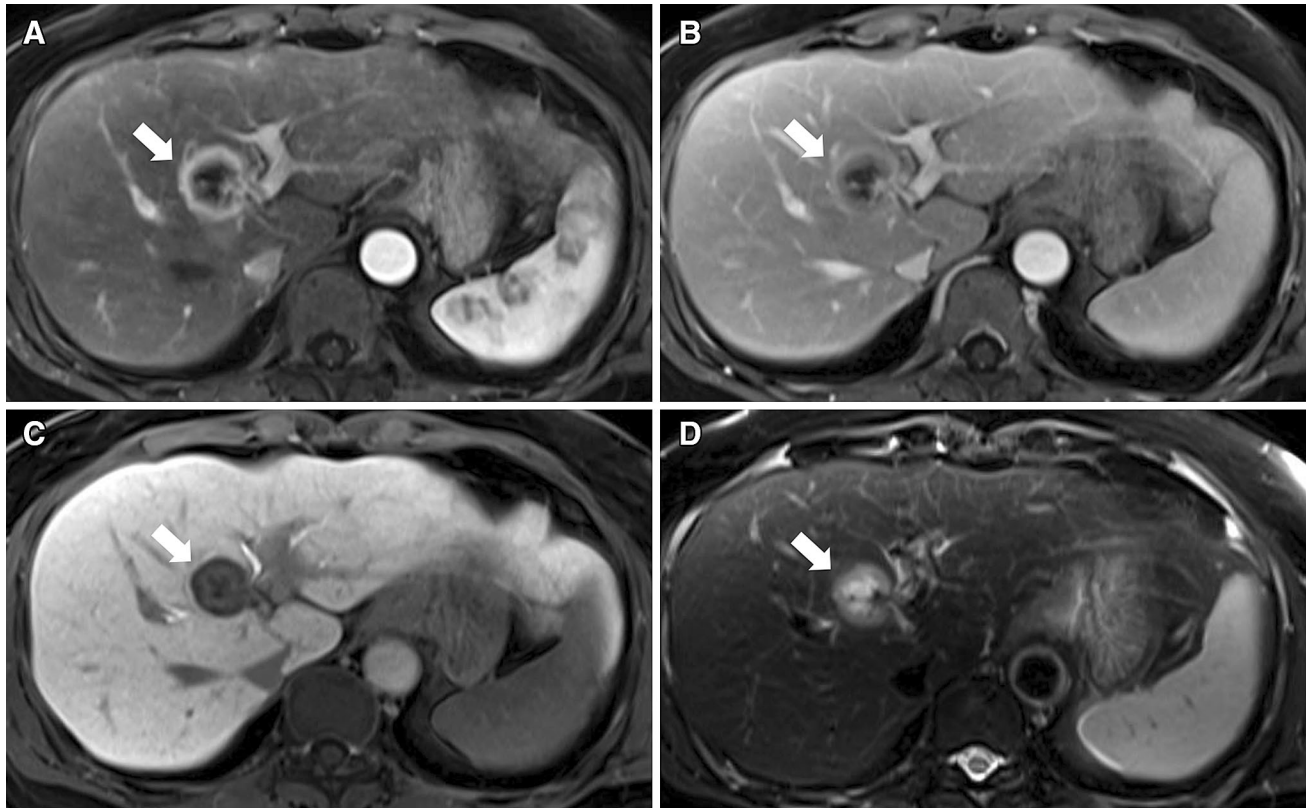


Fig. 2. A 2.7-cm sarcomatous hepatocellular carcinoma with hyaline degeneration and minimal tumor necrosis (1%) in a 64-year-old woman with hepatitis B-induced chronic hepatitis. Axial fat-suppressed T1-weighted 3D gradient echo images obtained during arterial phase (**A**) and portal venous phase (**B**): a round tumor (*arrows*) shows thick rim-like arterial

hyperenhancement with central hypointense area (*small arrow*). On 20-min HBP (**C**), the tumor (*arrow*) has a target appearance of central enhancing area with peripheral hypointense rim. On T2-weighted image (**D**), the tumor (*arrow*) shows a brighter central area than the peripheral tumor.

defect that might be mainly explained by central necrosis. Nonetheless, they were round or oval shaped as four tumors had a complete or partial capsule, characteristic of HCC. Interestingly, two S-HCCs with a thick hyperenhancing rim showed a target appearance on HBP and DWI, which could be explained by abundant collagen fiber in pathology. The imaging features of the remaining four sarcomatous tumors classified as neither S-HCC nor S-ICC were also dominated by abundant tumor necrosis: three tumors (carcinosarcoma or sarcomatous carcinoma) showed similar features to S-ICC and the remaining S-HCC-CC was a well-defined oval-shaped mass showing relatively thick peripheral arterial hyperenhancement, mimicking S-HCC.

On T2WI, liver malignancy is generally seen as moderately hyperintense, similar to the signal intensity of the spleen. According to the degree of necrosis or the presence of loose or dense fibrosis, ICC may show a darker or brighter area in the central portion of the tumor on T2WI [19]. Based on previous literature [13, 14] and our case series, extensive tumor necrosis in sarcomatous tumors produced a wide area of brighter T2

signal intensity similar to that of hemangioma or cyst; this feature was found in 10 of our cases. Interestingly, two S-ICCs and S-HCC-CC showed diffuse brightness on T2WI, mimicking hemangioma. This was not a typical presentation of a necrotic hepatic tumor. One S-ICC and one S-HCC also showed a central darker area on T2WI, which might be attributable to fibrosis.

We confirmed previous reports that sarcomatous carcinoma is prone to aggressive intrahepatic spreading and frequent metastasis or recurrence [1, 8, 15]. Of 18 tumors that were surgically resected, 17 showed macrovascular ($n = 7$) or microvascular ($n = 17$) invasion on pathology. On imaging, 10 tumors were accompanied by intrahepatic metastasis or tumor seeding. Two S-ICCs presented as subcapsular necrotic mass with rupture into the perihepatic space resulting in multifocal tumor seeding, similar to a prior report of ruptured S-HCC [25]. Fifteen patients who had undergone surgery showed recurrence that manifested as intrahepatic metastasis ($n = 9$), peritoneal seeding ($n = 9$), and metastasis to lymph node ($n = 5$), lung ($n = 3$), or bone ($n = 1$).

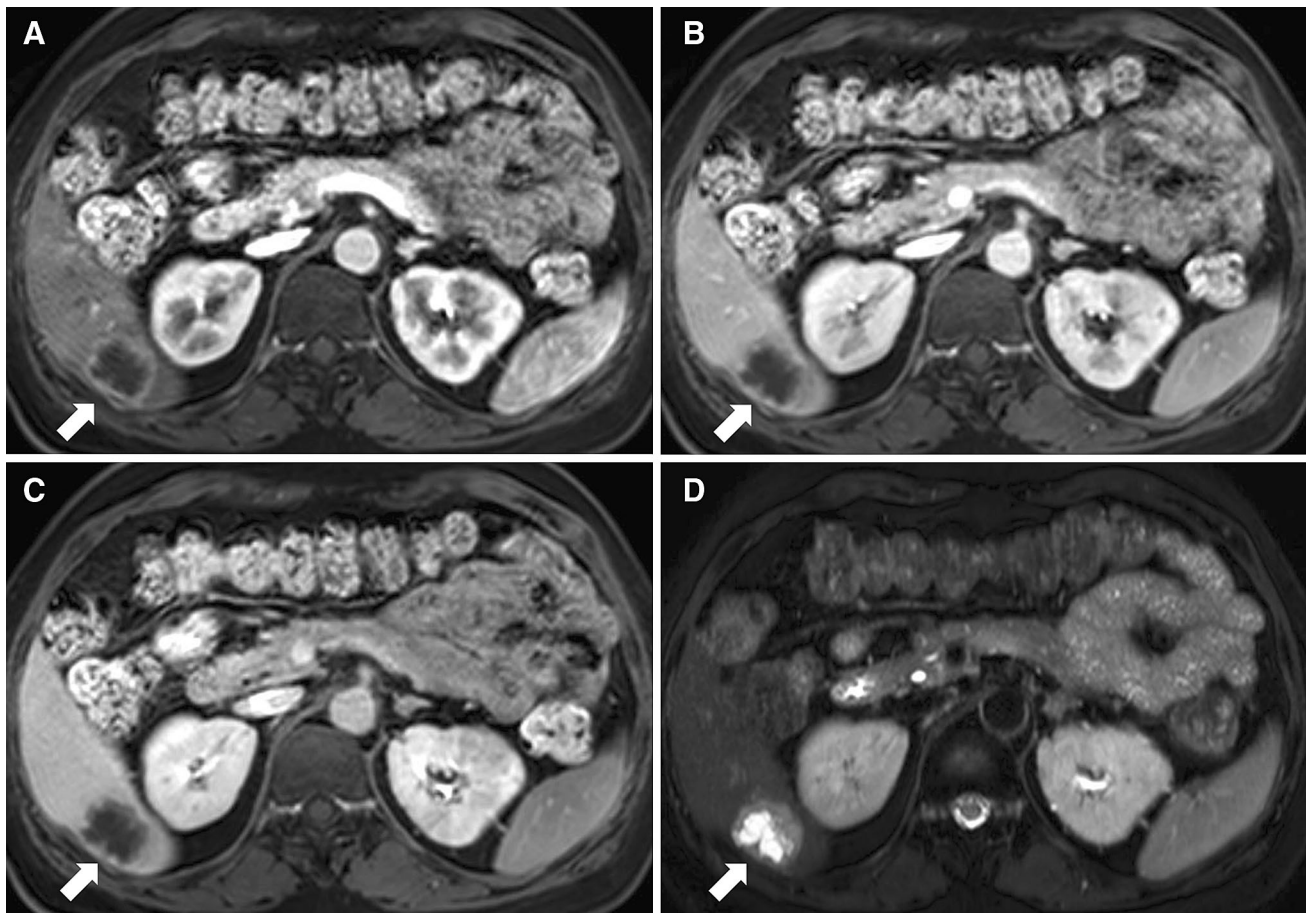


Fig. 3. A 4.5-cm sarcomatous intrahepatic cholangiocarcinoma with tumor necrosis (40%) in a 54-year-old woman with hepatitis B-induced chronic hepatitis. Axial fat-suppressed T1-weighted 3D gradient echo images obtained during arterial phase (**A**), portal venous phase (**B**), and 3-min delayed phase

(**C**): tumor with mildly lobulated contour (*arrows*) shows poor enhancement through dynamic phases. On T2-weighted image (**D**), the tumor (*arrow*) shows central bright signal intensity similar to that of fluid.

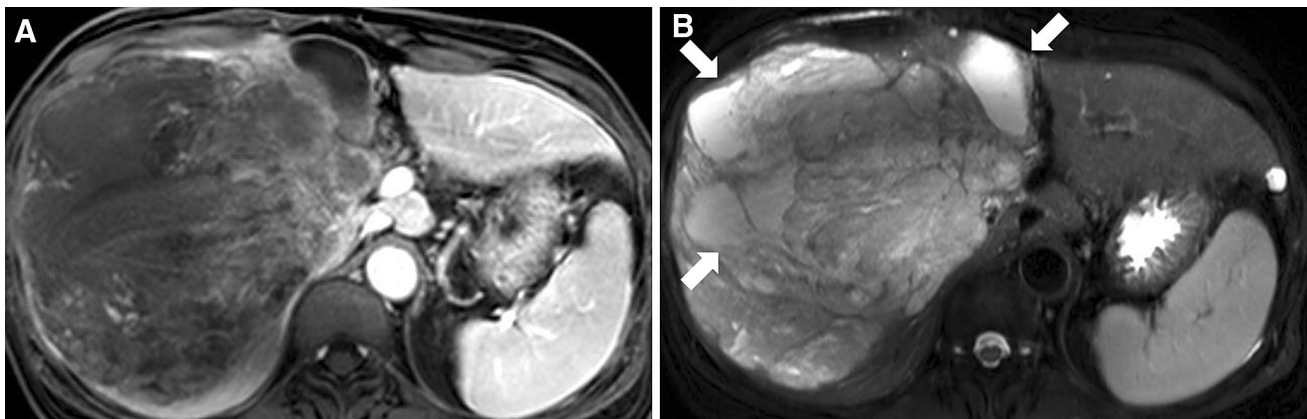


Fig. 4. A 23-cm sarcomatous intrahepatic cholangiocarcinoma with tumor necrosis (50%) in a 53-year-old man with hepatitis B-induced chronic hepatitis. Axial fat-suppressed T1-weighted 3D gradient echo images obtained during portal

venous phase (**A**) shows huge mass with minimal internal reticular enhancement. On T2-weighted image (**B**), most of the tumor (*arrow*) is seen as bright signal intensity similar to that of fluid with internal reticular signal intensities.

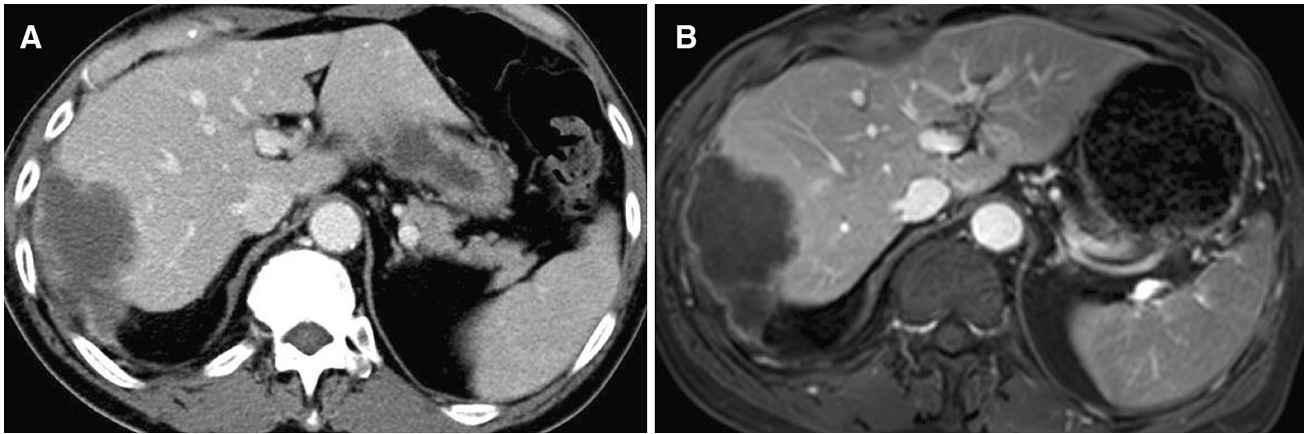


Fig. 5. A 7.5-cm sarcomatous intrahepatic cholangiocarcinoma in a 57-year-old man. The portal phase of multi-detector row CT (**A**) and fat-suppressed T1-weighted 3D

gradient echo image (**B**) shows an ill-defined subcapsular hypovascular hepatic mass that has ruptured into the perihepatic space.

Several limitations of this study should be noted. First, because this was a retrospective study, it may have some inherent selection bias. In addition, due to the retrospective nature of our study, a complete slice-by-slice matching between imaging and pathologic findings was not technically feasible. Thus, our explanations for the imaging features of tumors might be considered speculative. Second, our study is only descriptive for a selected case series without a control group. Consequently, we provided no statistical data on differential imaging features between sarcomatous tumor and other hepatic tumors.

In conclusion, hepatic sarcomatous carcinoma including S-HCC and S-ICC generally presents as minimal rim-like arterial enhancement or extreme hypovascularity on CT and gadoxetic acid-enhanced MRI with a high frequency of T2 bright area due to extensive tumor necrosis and vascular invasion.

Compliance with ethical standards

Funding No funding was received for this study.

Conflict of interest All authors declare that they have no conflict of interest.

Ethical approval All procedures performed in studies involving human participants were in accordance with the ethical standards of the institutional and/or national research committee and with the 1964 Helsinki declaration and its later amendments or comparable ethical standards. For this type of study formal consent is not required.

Informed consent Statement of informed consent was not applicable since the manuscript does not contain any patient data.

References

- Kakizoe S, Kojiro M, Nakashima T (1987) Hepatocellular carcinoma with sarcomatous change. Clinicopathologic and immunohistochemical studies of 14 autopsy cases. *Cancer* 59:310–316
- Nishi H, Taguchi K, Asayama Y, et al. (2003) Sarcomatous hepatocellular carcinoma: a special reference to ordinary hepatocellular carcinoma. *J Gastroenterol Hepatol* 18:415–423
- Nakajima T, Tajima Y, Sugano I, et al. (1993) Intrahepatic cholangiocarcinoma with sarcomatous change. Clinicopathologic and immunohistochemical evaluation of seven cases. *Cancer* 72:1872–1877
- Watanabe G, Uchinami H, Yoshioka M, Nanjo H, Yamamoto Y (2014) Prognosis analysis of sarcomatous intrahepatic cholangiocarcinoma from a review of the literature. *Int J Clin Oncol* 19:490–496. doi:10.1007/s10147-013-0586-x
- Kaibori M, Kawaguchi Y, Yokoigawa N, et al. (2003) Intrahepatic sarcomatoid cholangiocarcinoma. *J Gastroenterol* 38:1097–1101. doi:10.1007/s00535-003-1203-y
- Sumiyoshi S, Kikuyama M, Matsubayashi Y, et al. (2007) Carcinosarcoma of the liver with mesenchymal differentiation. *World J Gastroenterol* 13:809–812
- Tsou YK, Wu RC, Hung CF, Lee CS (2008) Intrahepatic sarcomatoid cholangiocarcinoma: clinical analysis of seven cases during a 15-year period. *Chang Gung Med J* 31:599–605
- Malhotra S, Wood J, Mansy T, et al. (2010) Intrahepatic sarcomatoid cholangiocarcinoma. *J Oncol* 2010:701476. doi:10.1155/2010/701476
- Hamilton SR, Aaltonen LA (2000) *Pathology and genetics of tumours of the digestive system*. Lyon: IARC press
- Lin YS, Wang TY, Lin JC, et al. (2013) Hepatic carcinosarcoma: clinicopathologic features and a review of the literature. *Ann Hepatol* 12:495–500
- Schneider G, Massmann A, Fries P, Kramann B, Remberger K (2005) MRI of sarcomatoid carcinoma of the liver. *Eur J Radiol Extra* 54:63–67. doi:10.1016/j.ejrex.2005.03.008
- Honda H, Hayashi T, Yoshida K, et al. (1996) Hepatocellular carcinoma with sarcomatous change: characteristic findings of two-phased incremental CT. *Abdom Imaging* 21:37–40
- Bilgin M, Toprak H, Bilgin SS, Kondakci M, Balci C (2012) CT and MRI findings of sarcomatoid cholangiocarcinoma. *Cancer Imaging* 12:447–451. doi:10.1102/1470-7330.2012.0036
- Yasutake T, Kiryu S, Akai H, et al. (2014) MR imaging of carcinosarcoma of the liver using Gd-EOB-DTPA. *Magn Reson Med* 13:117–121. doi:10.2463/mrms.2013-0011
- Kojiro M, Sugihara S, Kakizoe S, Nakashima O, Kiyomatsu K (1989) Hepatocellular carcinoma with sarcomatous change: a special reference to the relationship with anticancer therapy. *Cancer Chemother Pharmacol* 23(Suppl):S4–8
- Shimada M, Takenaka K, Rikimaru T, et al. (2000) Characteristics of sarcomatous cholangiocarcinoma of the liver. *Hepatogastroenterology* 47:956–961
- Hwang S, Lee SG, Lee YJ, et al. (2008) Prognostic impact of sarcomatous change of hepatocellular carcinoma in patients undergoing liver resection and liver transplantation. *J Gastrointest Surg* 12:718–724. doi:10.1007/s11605-007-0393-7
- Park HJ, Kim YK, Park MJ, Lee WJ (2013) Small intrahepatic mass-forming cholangiocarcinoma: target sign on diffusion-weighted

- ted imaging for differentiation from hepatocellular carcinoma. *Abdom Imaging* 38:793–801. doi:[10.1007/s00261-012-9943-x](https://doi.org/10.1007/s00261-012-9943-x)
19. Chong YS, Kim YK, Lee MW, et al. (2012) Differentiating mass-forming intrahepatic cholangiocarcinoma from atypical hepatocellular carcinoma using gadoxetic acid-enhanced MRI. *Clin Radiol* 67:766–773. doi:[10.1016/j.crad.2012.01.004](https://doi.org/10.1016/j.crad.2012.01.004)
 20. Ishigami K, Yoshimitsu K, Nishihara Y, et al. (2009) Hepatocellular carcinoma with a pseudocapsule on gadolinium-enhanced MR images: correlation with histopathologic findings. *Radiology* 250:435–443. doi:[10.1148/radiol.2501071702](https://doi.org/10.1148/radiol.2501071702)
 21. Eisenhauer E, Therasse P, Bogaerts J, et al. (2009) New response evaluation criteria in solid tumours: revised RECIST guideline (version 1.1). *Eur J cancer* 45:228–247
 22. Yu RS, Chen Y, Jiang B, Wang LH, Xu XF (2008) Primary hepatic sarcomas: CT findings. *Eur Radiol* 18:2196–2205. doi:[10.1007/s00330-008-0997-7](https://doi.org/10.1007/s00330-008-0997-7)
 23. Pua U, Low SC, Tan YM, Lim KH (2009) Combined hepatocellular and cholangiocarcinoma with sarcomatoid transformation: radiologic-pathologic correlation of a case. *Hepatol Int* 3:587–592. doi:[10.1007/s12072-009-9150-1](https://doi.org/10.1007/s12072-009-9150-1)
 24. Koo HR, Park MS, Kim MJ, et al. (2008) Radiological and clinical features of sarcomatoid hepatocellular carcinoma in 11 cases. *J Comput Assist Tomogr* 32:745–749. doi:[10.1097/RCT.0b013e3181591ccd](https://doi.org/10.1097/RCT.0b013e3181591ccd)
 25. Hung Y, Hsieh TY, Gao HW, Chang WC, Chang WK (2014) Unusual computed tomography features of ruptured sarcomatous hepatocellular carcinoma. *J Chin Med Assoc* 77:265–268. doi:[10.1016/j.jcma.2014.02.006](https://doi.org/10.1016/j.jcma.2014.02.006)
 26. Idobe-Fujii Y, Ogi N, Hoshio K, et al. (2006) Hepatocellular carcinoma with sarcomatous change arising after eradication of HCV via interferon therapy. *Clin Imaging* 30:416–419. doi:[10.1016/j.clinimag.2006.07.004](https://doi.org/10.1016/j.clinimag.2006.07.004)
 27. Inoue Y, Lefor AT, Yasuda Y (2012) Intrahepatic cholangiocarcinoma with sarcomatous changes. *Case Rep Gastroenterol* 6:1–4. doi:[10.1159/000335883](https://doi.org/10.1159/000335883)
 28. Giunchi F, Vasuri F, Baldin P, et al. (2013) Primary liver sarcomatous carcinoma: report of two cases and review of the literature. *Pathol Res Pract* 209:249–254. doi:[10.1016/j.prp.2013.01.005](https://doi.org/10.1016/j.prp.2013.01.005)
 29. Haratake J, Yamada H, Horie A, Inokuma T (1992) Giant cell tumor-like cholangiocarcinoma associated with systemic cholelithiasis. *Cancer* 69:2444–2448